

On streak breakdown in bypass transition

Philipp Schlatter,¹ Luca Brandt,¹ H. C. de Lange,² and Dan S. Henningson¹

¹Linné Flow Centre, KTH Mechanics, SE-100 44 Stockholm, Sweden

²Department of Mechanical Engineering, Eindhoven University of Technology, NL-5600 Eindhoven, The Netherlands

(Received 10 December 2007; accepted 29 May 2008; published online 31 October 2008)

Recent theoretical, numerical, and experimental investigations performed at the Department of Mechanics, KTH Stockholm, and the Department of Mechanical Engineering, Eindhoven University of Technology, are reviewed, and new material is presented to clarify the role of the boundary-layer streaks and their instability with respect to turbulent breakdown in bypass transition in a boundary layer subject to free-stream turbulence. The importance of the streak secondary-instability process for the generation of turbulent spots is clearly shown. The secondary instability manifests itself as a growing wave packet located on the low-speed streak, increasing in amplitude as it is dispersing in the streamwise direction. In particular, qualitative and quantitative data pertaining to temporal sinuous secondary instability of a steady streak, impulse responses both on a parallel and a spatially developing streak, a model problem of bypass transition, and full simulations and experiments of bypass transition itself are collected and compared. In all the flow cases considered, similar characteristics in terms of not only growth rates, group velocity, and wavelengths but also three-dimensional visualizations of the streak breakdown have been found. The wavelength of the instability is about an order of magnitude larger than the local boundary-layer displacement thickness δ^* , the group velocity about 0.8 of the free-stream velocity U_∞ , and the growth rate on the order of a few percent of U_∞/δ^* . The characteristic structures at the breakdown are quasistreamwise vortices, located on the flanks of the low-speed region arranged in a staggered pattern. © 2008 American Institute of Physics. [DOI: 10.1063/1.3005836]

I. INTRODUCTION

Transition in boundary layers exposed to moderate to high levels of free-stream turbulence, termed bypass transition, has in recent years been studied by a number of authors. This transition scenario is dominated by the—randomly in space and time—appearance of streamwise elongated structures in the boundary layer with alternating positive and negative streamwise disturbance velocities, the so-called streaks. The amplitude of the boundary-layer disturbance grows in the downstream direction, and finally—through a rapid process bypassing the exponential growth of Tollmien–Schlichting waves—breakdown into localized turbulent spots occurs. These spots also increase in size and merge until a fully turbulent boundary layer can be observed. Andersson *et al.*¹ have computed optimally growing streaks and showed that the streaks preceding the breakdown to turbulence have the same characteristics as the optimal disturbances. Based on the Reynolds-number scaling of the optimal growth, they found a model which could determine the dependence of the transition location on the Reynolds number. Zaki and Durbin² used a parallel-flow model and considered the growth of the streaks as forcing of the Squire modes from Orr–Sommerfeld modes, using the type of eigenfunction expansions discussed by Henningson and Schmid.³ The first direct numerical simulation (DNS) of bypass transition was performed by Jacobs and Durbin,⁴ who found good overall agreement with the experiments of Roach and Brierley.⁵ Further numerical simulations have been performed by Brandt *et al.*⁶ and Nagarajan *et al.*,⁷ and recent experiments by Mat-

subara and Alfredsson⁸ and Mans *et al.*^{9,10} For additional references see the book by Schmid and Henningson¹¹ and the recent review by Durbin and Wu.¹²

From the previous work, there is a consensus about the overall features of the bypass-transition process. Free-stream vortical disturbances enter the boundary layer, mainly at the leading-edge area, where their streamwise vorticity components induce transiently growing streamwise streaks by the lift-up effect. The streaks break down locally and growing turbulent spots appear. The spots subsequently merge causing a fully developed turbulent boundary layer further downstream. However, the cause of the breakdown into turbulent spots has generated some controversy, something we aim at clarifying in this paper.

In the experiments by Mans¹³ (also reported in Mans *et al.*¹⁰) the initiation of the streak breakdown in bypass transition has been studied in detail. In Fig. 1, two typical routes of breakdown are visualized via dye injected in the experimental apparatus. In the sequence on the left a sinuous or antisymmetric breakdown is seen to develop, and in the sequence on the right a breakdown involving a varicose or symmetric oscillations of the streaks is shown.

Detailed experiments on the streak breakdown were also performed under controlled conditions by Litvinenko *et al.*¹⁴ for two-dimensional boundary layers; in particular, they were able to identify flow structures in close agreement with those obtained numerically by Brandt and Henningson¹⁵ for sinuous secondary instability of boundary-layer streaks. Additionally, Chernoray *et al.*¹⁶ examined the secondary instabil-

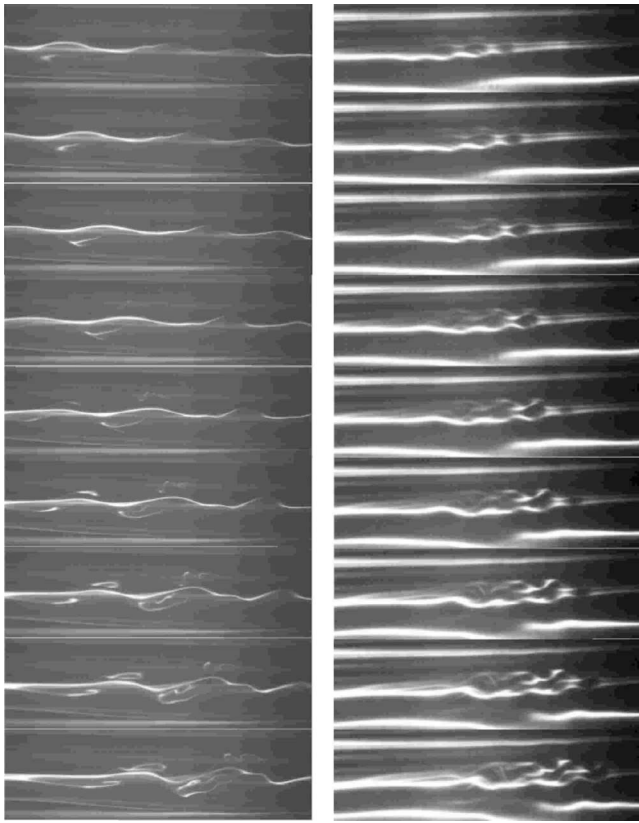


FIG. 1. Dye visualization of bypass transition in the experiments. Two different streak breakdown sequences developing on a low-speed streak are shown. Left column: Sinuous antisymmetric breakdown. Right column: Varicose symmetric breakdown. From J. Mans, Ph.D. thesis, Eindhoven University of Technology (2007); courtesy of Mans and de Lange.

ity of crossflow modes in three-dimensional boundary layers and their connection to the two-dimensional (unswept) case.

Similar structures have also been identified in the numerical simulations of bypass transition by Brandt *et al.*;⁶ two typical (sinuous and varicose) structures taken from

these numerical simulations are depicted in Fig. 2 showing isocontours of both disturbance velocity and the λ_2 vortex identification criterion.¹⁷ In both the simulations and experiments the sinuous breakdown is more common, and we will consider the disturbances with this symmetry in detail in this paper. The aim is to show that the flow structures seen in Figs. 1 and 2 result from a secondary instability of the underlying streaks. First, we study both a linear and a nonlinear impulse response on saturated optimal streaks, and extract quantitative information from the developing wave packet, in particular, propagation speeds, growth rates, and wavelengths. Second, we consider a model recently proposed by Zaki and Durbin² which they have shown to be a suitable approximation of the full bypass-transition scenario. From the calculation of their model we obtain the characteristics of the secondary-instability wave packets causing transition to turbulence in that case. Finally, we compare in more detail to secondary-instability characteristics taken from the simulations by Brandt and Henningson.¹⁵ We show that the characteristics of all these secondary-instability wave packets agree, and can thus be assumed to have the same origin.

II. NUMERICAL AND EXPERIMENTAL METHOD

In this work, we present results obtained both numerically and experimentally. A short description of the numerical method and the experimental setup is given in this section. Further information on exact details is directly mentioned throughout the text whenever necessary.

A. Numerical technique

The simulation code (see Chevalier *et al.*¹⁸) employed for the simulations presented here uses spectral methods to solve the three-dimensional time-dependent incompressible Navier–Stokes equations over a flat plate. The streamwise, wall-normal, and spanwise directions are denoted by x , y , and z , respectively, and the corresponding velocity vector is

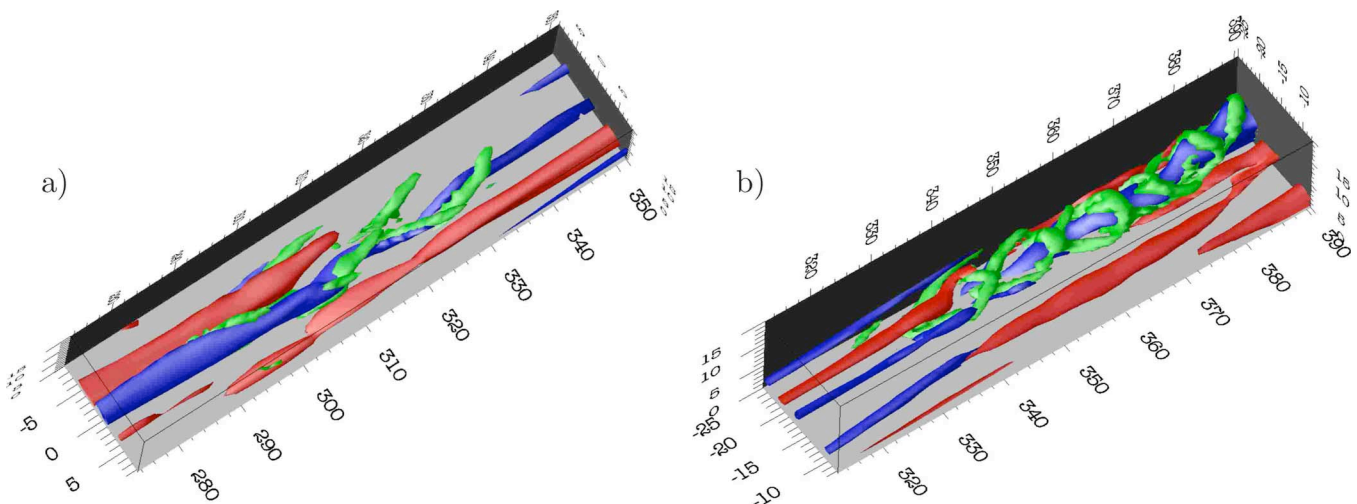


FIG. 2. (Color online) Three-dimensional visualization of the numerical simulations of bypass transition pertaining to two different types of structures prior to the formation of a turbulent spot. (a) Sinuous breakdown. (b) Varicose breakdown. Isocontours of positive and negative streamwise disturbance velocities $\pm u' = 0.15$ in medium (red) and dark gray (blue) isocontours, respectively, and light gray (green) surfaces of the λ_2 vortex identification criterion (Ref. 17) ($\lambda_2 = -0.002$).

$\mathbf{u}=(u,v,w)^T$. The algorithm is based on Fourier discretization in the streamwise and spanwise directions and an expansion in Chebyshev polynomials in the wall-normal direction. The nonlinear convection terms are evaluated pseudospectrally in physical space using fast Fourier transforms. Aliasing errors from the evaluation of the nonlinear terms are removed by the 3/2-rule in the wall-parallel x/z plane. In the wall-normal direction, it has been found more convenient to increase resolution rather than to use dealiasing. The time is advanced using a four-step low-storage third-order Runge–Kutta method for the nonlinear and forcing terms and a second-order Crank–Nicolson method for the linear terms. The code is fully parallelized for efficient use on both shared- and distributed-memory systems.

To correctly account for the downstream growth of the boundary layer, a spatial technique is necessary. This requirement is combined with the periodic boundary conditions in the streamwise direction by adding a fringe region, similar to that described by Bertolotti *et al.*¹⁹ In this region, located at the downstream end of the computational box, the function $\lambda(x)$ in Eq. (1) is smoothly raised from zero and the flow is forced to a desired solution \mathbf{v} in the following manner:

$$\frac{\partial \mathbf{u}}{\partial t} + (\mathbf{u} \cdot \nabla) \mathbf{u} = -\nabla p + \frac{1}{\text{Re}_{\delta_0^*}} \nabla^2 \mathbf{u} + \lambda(x)(\mathbf{v} - \mathbf{u}), \quad (1)$$

$$\nabla \cdot \mathbf{u} = 0, \quad (2)$$

with the pressure p . The desired in- and outflow velocity vector \mathbf{v} may depend on the three spatial coordinates and time. It is smoothly changed from the laminar boundary-layer profile at the beginning of the fringe region to the prescribed inflow velocity vector. This is normally a laminar boundary-layer profile, but may also contain desired inflow disturbances.

All quantities are nondimensionalized using the (constant) free-stream velocity U_∞ , the viscosity ν , and the displacement thickness at the inlet δ_0^* ($x=0$). The computational Reynolds number is thus $\text{Re}_{\delta_0^*} = U_\infty \delta_0^* / \nu$. For the undisturbed Blasius solution, the 99%-boundary-layer thickness $\delta_{99} \approx 2.85 \delta^*$.

B. Experimental technique

At the Technische Universiteit Eindhoven (TU/e) an experimental setup has been developed to study the flow phenomena during natural (no added triggering) bypass transition. This means that streaks are generated by exposing the experimental boundary layer to grid-generated free-stream turbulence.

The basic components of the experimental setup are two cylindrical reservoirs of 2 m height, with a cross section of 1.2 m as described by Mans.¹³ They are interconnected by an optically accessible measuring section, made of glass, which is 2.7 m long, 0.57 m wide, and 0.45 m high. A network of pumps and pipelines, situated between the reservoirs, provides the circulation of the water from the inflow reservoir through the measuring section to the outflow reservoir. The bypass transition is generated by exposing the experimental boundary layer to grid-generated free-stream turbulence. The

turbulence characteristics above the leading edge of the plate are:¹³ Turbulence intensity $Tu=5.8\%$, streamwise root-mean-square (rms) fluctuation $u_{\text{rms}}/\nu=5 \times 10^3 \text{ m}^{-1}$, integral length scale $\text{Re}_L=125$, Taylor scale $\text{Re}_\lambda=25$, and Kolmogorov scale $\text{Re}_\eta=3.5$. A characteristic value of the boundary-layer thickness is $\delta^*=2.4 \text{ mm}$ at $\text{Re}_{\delta^*}=300$.

The combined particle image velocimetry (PIV)-laser induced fluorescence (LIF) technique proposed by Ren *et al.*²⁰ is utilized in a horizontal laser sheet, with two cameras mounted above the water channel. The thickness of the laser sheet is set by means of a diaphragm which is positioned behind the negative lens and is chosen to be 4 mm. The position of the center of the sheet is set to approximately 5 mm above the plate. For the PIV, polyamide seeding particles with a diameter of 20 μm are added to the system. The scattered light from the particles when illuminated by a Nd:YAG (yttrium aluminum garnet) laser sheet (wavelength $\lambda=532 \text{ nm}$) is recorded by a charge coupled device (CCD) camera (Kodak Megaplus 1008 \times 1018 pixel, 10 bits). Single exposed images are recorded. PIV image pairs (consisting of two single exposed images) are recorded with a frequency of 14.8 Hz. For the visualizations the same LIF technique as described in Mans *et al.*⁹ is used. The fluorescent dye Rhodamine B is inserted into the boundary layer. The dye inlet is located at 0.19 m from the leading edge and consists of a spanwise row of holes with diameter of $1 \times 10^{-3} \text{ m}$, positioned with an intermediate distance of $1 \times 10^{-2} \text{ m}$. The dye streaklines are excited by the laser sheet and will therefore emit fluorescent light that is captured by the second CCD camera. The camera mounted perpendicular to the flow is the PIV camera, while the oblique one is the visualization camera. The lens of the PIV CCD camera is provided with a filter, which only allows light to pass with wavelength of 532 nm, this to block light from the dye streaklines in the PIV recordings. A holographic notch filter is mounted on the lens of the LIF CCD camera to block the light coming from the Nd:YAG laser. The oblique configuration of the cameras enables a maximum overlap between the PIV and visualization-recording areas. Both recording areas are calibrated using a technique described by Kieft *et al.*²¹ In Mans *et al.*¹⁰ the evolution of the flow structures during the bypass-transition process is observed while moving the cameras and laser-sheet optics along with the flow with a velocity of 0.09 m/s in a downstream direction. This velocity equals the average velocity of flow structures at the measurement height. The output of one experimental run consists of the visualizations of the dye streaklines and the corresponding instantaneous velocity fields. The “typical” sinuous motion of the unstable streak in the dye visualizations¹³ is used to identify the velocity fields in which a sinuous instability develops.

III. SINUOUS STREAK BREAKDOWN

A. Streak formation

The occurrence of low-frequency streamwise elongated structures as response of the boundary layer to free-stream vortical modes was first documented by Klebanoff.²² However, early studies by Taylor already reported on the modu-

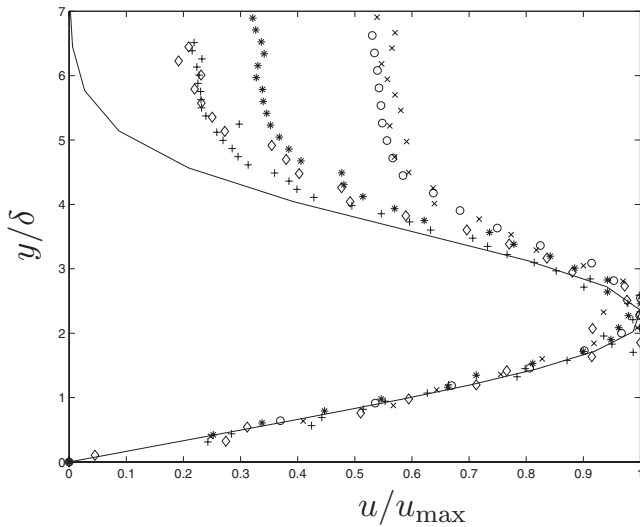


FIG. 3. Wall-normal profile of the streamwise velocity disturbance for the optimal spatial transient growth in comparison with the experiments by Westin *et al.* (Ref. 24). The wall-normal coordinate y is scaled with $\delta = 0.581\delta^*$. Adapted from Andersson *et al.* (Ref. 26).

lations of the boundary layer induced in noisy environments. The formation of low-frequency oscillations was further investigated by Kendall²³ who denoted these streaks as Klebanoff modes. It is now well understood that the growth of the streaks can be successfully explained by the theory of nonmodal growth.¹ Physically, the streaks are the results of the tilting of the spanwise vorticity associated with the mean boundary-layer flow by perturbation varying in the spanwise direction, elongated streamwise vortices being the most effective owing to their lower decay rate. In Fig. 3 it is shown that the wall-normal mode shape of the optimal disturbance found in the theoretical works¹ is remarkably similar to the streamwise u_{rms} fluctuation values measured in boundary layers exposed to free-stream turbulence.²⁴ The maximum fluctuation level is achieved in the middle of the boundary layer at a distance from the wall $y/\delta^* = 1.3$. The spanwise correlation of the streamwise velocity perturbations reported by Matsubara and Alfredsson⁸ shows that the spanwise scale of the streaks is of the order of the boundary-layer thickness, in full agreement with previous theoretical work on the transient growth in spatially evolving boundary layers. Further, the experiments show that the wall-normal maximum of the streamwise velocity fluctuations $u_{\text{rms,max}}^2$ grows linearly with the Reynolds number based on the distance from the leading edge Re_x , again in full agreement with the theoretical predictions. Andersson *et al.*¹ proposed a transition-prediction model based on optimal growth calculations, where it is observed that $u_{\text{rms,max}} \propto Re_x^{1/2} Tu$ with the turbulence intensity Tu . Assuming that transition occurs when the level of streamwise velocity fluctuations reaches a given threshold, roughly at the amplitudes at which the streaks become unstable, the transition location Re_T can be related to the turbulence intensity by $Re_T Tu^2 = \text{const}$. The model was validated against experimental results by Matsubara *et al.*,²⁵ showing good correlation between transition location and the level of the free-stream turbulence only based on results of nonmodal growth.

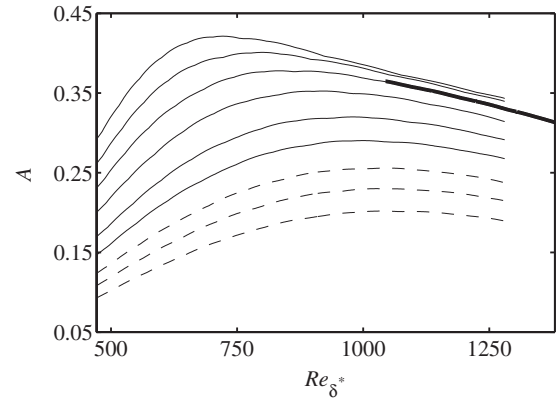


FIG. 4. Nonlinear development of the optimal streaks. The dashed lines indicate linearly stable streaks, whereas the thick solid line represents the amplitude of the streaky flow used for the simulation of the nonlinear impulse response in Sec. III C.

To study the breakdown in boundary layers exposed to free-stream turbulence, steady spanwise-periodic optimal streaks are therefore used as a model. The results obtained assuming steady periodic streaks are quantitatively compared with simulations and experiments of boundary layers exposed to free-stream turbulence to clarify the role of the streak instability in the transition process. Streaks of critical amplitudes were computed by Andersson *et al.*²⁶ These authors used the optimal disturbance as inlet profile in the DNS of a spatially evolving zero-pressure-gradient boundary layer. The nonlinear development of the optimal streaks at different inlet disturbance levels is displayed in Fig. 4, where the streak amplitude is defined as

$$A = \frac{1}{2} \left\{ \max_{y,z} [U(y,z) - U_B(y)] - \min_{y,z} [U(y,z) - U_B(y)] \right\}, \quad (3)$$

with U_B being the laminar Blasius profile. Linearly stable streak profiles are indicated with dashed lines in the plot, whereas the thick line represents the initial field used for the numerical simulations of the streak impulse response presented in Sec. III C.

B. Secondary instabilities of the optimal streaks

In this section the main findings from the linear secondary instability of streak profiles under the parallel-flow assumption are revisited. The frozen streak is justified since the instability is inviscid in nature and therefore leads to fast streamwise growth, whereas the streak obeys the boundary-layer approximation and is thus slowly varying downstream. The secondary instabilities and breakdown of the optimal streamwise streaks were studied by Andersson *et al.*,²⁶ Brandt *et al.*,²⁷ and Brandt and Henningson.¹⁵

Since the streak instability is of inflectional nature, Andersson *et al.*²⁶ performed an inviscid stability analysis. The results indicate that sinuous antisymmetric perturbations are the most dangerous, with critical threshold amplitude of about 26% of the free-stream velocity. This instability is related to an inflection point in the spanwise direction. Conversely, varicose symmetric waves, the result of wall-normal inflectional profiles, are found to become unstable for streak

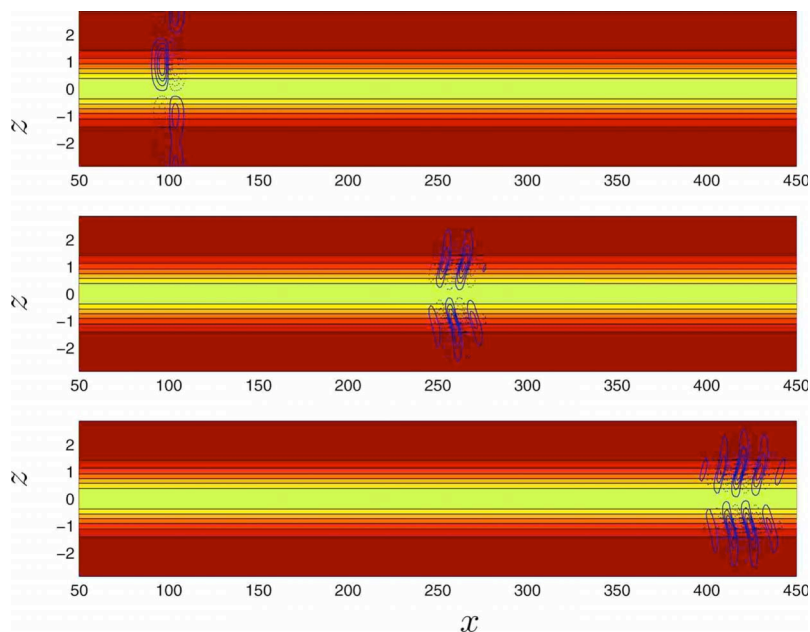


FIG. 5. (Color online) Development of the linear impulse response on a parallel streak in a wall-parallel plane ($y=1.8$) for three different times $t=0$, $t=200$, $t=400$. The background color represents the streamwise velocity of the base flow, with high to lower velocity ranging from dark (red) to light (yellow). The isolines indicate the wall-normal perturbation velocity; dotted lines denote negative values. From L. Brandt, Ph.D. thesis, KTH Stockholm (2003) (Ref. 30).

amplitudes larger than 37% of the free-stream velocity. Note, however, that Hoepffner *et al.*,²⁸ following the work by Schoppa and Hussain,²⁹ showed that nonlinearly saturated optimal streaks can experience significant transient growth at subcritical amplitudes, leading to turbulent breakdown. The critical threshold identified by linear stability analysis can therefore be a too conservative estimate for the streak amplitude at transition. The results on the nonmodal growth of secondary waves reveal that the sinuous modes are again those subject to the largest transient amplification; however, the growth of varicose perturbations is significant already at amplitudes of about 20%. Interestingly, the shape of the perturbations arising as a result of the nonmodal amplification is very similar to that of the most unstable linear modes. It is therefore concluded by Hoepffner *et al.*²⁸ that it would be virtually impossible to distinguish between the two scenarios, modal and nonmodal, from experiments and simulations of bypass transition.

Brandt *et al.*²⁷ studied the secondary instability by considering the impulse response of a frozen streak. The development of the linear perturbations evolving on the streaks from the simulations is displayed in Fig. 5. The figure shows how an asymmetric localized initial condition evolves into an antisymmetric wave packet. From such simulations the spatiotemporal instability characteristics can be found; as an example, the temporal stability of the streak profile with amplitude $A=0.36$ is reported in Fig. 6 where the inviscid results from Ref. 26 are also displayed for comparison. The streaks are found to be convectively unstable; the group velocity of the most unstable waves is about 0.8, while the trailing and leading edges of the unstable wave packets travel at about 0.65 and 0.95 of the free-stream velocity, respectively.

C. Nonlinear impulse response

Numerical simulations of the nonlinear impulse response are performed with a twofold motivation. First, we aim at comparing the structures and scales at the breakdown to those predicted by the linear analysis. Second, the scenario likely to occur in bypass transition takes the form of a propagating wave packet. Note that, unlike the simulations in Ref. 15, the perturbation is introduced as a localized initial condition and not induced by a continuous harmonic forcing at the upstream inlet. As a consequence, the perturbation evolves in the form of a wave packet. Further, the underlying streak is not assumed to be parallel but slowly decaying in the streamwise direction, see Fig. 4.

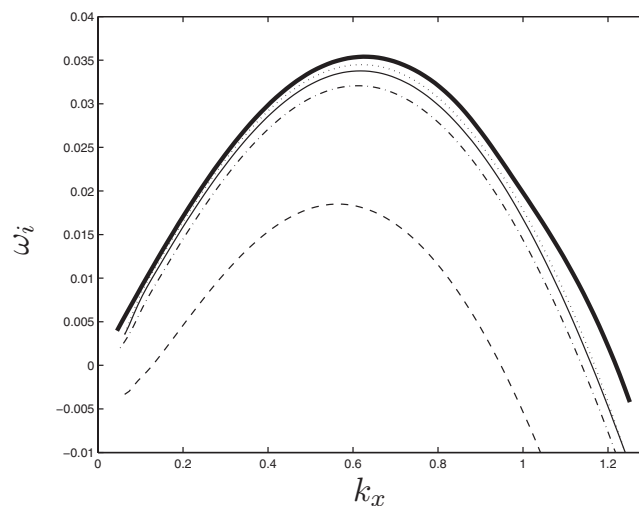


FIG. 6. Temporal growth rate ω_i vs streamwise wavenumber k_x , determined from the linear impulse response for various Reynolds numbers (\cdots : $Re=2000$; $—$: $Re=1047$; $- \cdot -$: $Re=500$; $- - -$: $Re=100$) and the inviscid limit ($—$). The streak amplitude is $A=0.36$. From L. Brandt, Ph.D. thesis, KTH Stockholm (2003) (Ref. 30).

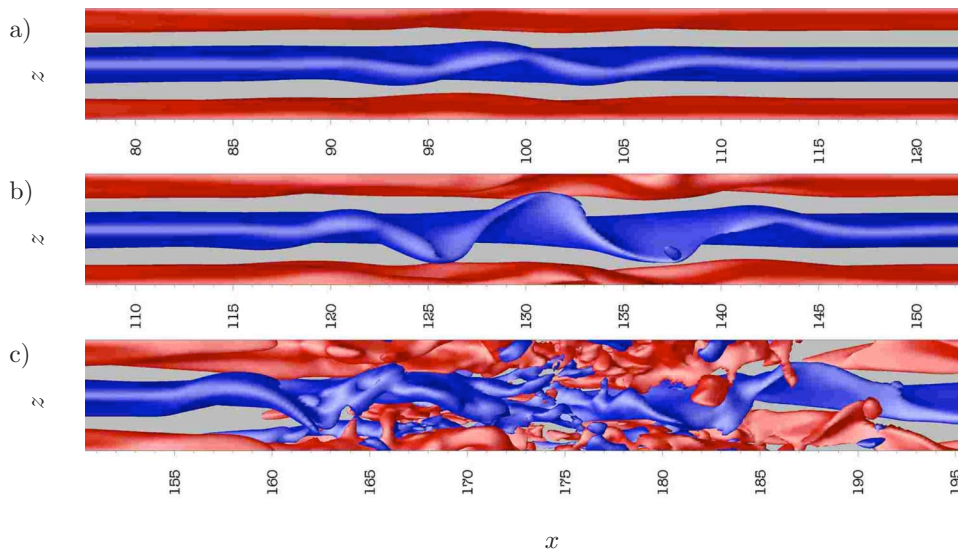


FIG. 7. (Color online) Top view of the flow development for the nonlinear impulse response on a spatially evolving streak at times (a) $t=120$, (b) $t=160$, and (c) $t=220$. Low-speed streaks are indicated by dark gray (blue) isocontours; medium gray (red) isocontours correspond to high-speed streaks ($u' = \pm 0.12$).

To study the consequence of high-frequency actuation on the development of a nonlinear streak, an artificial initial condition is used to excite the streak and to initiate the impulse response. As opposed to the real “situation” in bypass transition where this excitement is connected to the receptivity of the boundary layer to free-stream turbulence,^{2,31} the present condition consists of many wavenumbers and it is located close to the wall. The following initial condition, defined in terms of the stream function ψ , is used:

$$\psi(x, y, z; 0) = -A_\epsilon \bar{x} \bar{y}^3 \bar{z} \exp(-\bar{x}^2 - \bar{y}^2 - \bar{z}^2), \quad (4)$$

where $\bar{x} = (x - x_0)/l_x$, $\bar{y} = y/l_y$, and $\bar{z} = (z - z_0)/l_z$. The velocity components of the disturbance are obtained as $u' = 0$, $v' = \partial\psi/\partial z$, and $w' = -\partial\psi/\partial y$ from the vector potential $(\psi, 0, 0)$. The amplitude A_ϵ is set to 0.03. The length scales, $l_x = 2.5$, $l_y = 1$, and $l_z = 0.8$ have been chosen small enough to reproduce a localized impulse within the limits of a good resolution in the truncated spectral space of the numerical simulations. Additionally, the spanwise length scale is small compared to the width of the computational domain such that the disturbance amplitude is vanishing across the periodic

boundaries; the no-slip boundary condition at the wall is fulfilled due to the factor \bar{y}^3 in Eq. (4). The disturbance is centered around $x_0 = 5$ and $z_0 = 1.3$, which is chosen to lie off axis in one of the two regions of strongest spanwise shear so that no particular symmetry is enforced on the solution. The initial condition (4) consists of two counter-rotating streamwise vortex pairs. It has been used previously in Refs. 32 and 33 and almost in the same form in Ref. 34.

Instantaneous flow visualizations of the flow response are reported in Figs. 7 and 8. Figure 7 displays a top view of three-dimensional surfaces of constant streamwise velocity perturbation $u' = \pm 0.12$ at three different time instances. The streamwise velocity perturbation is defined as the difference between the actual value of the velocity and its instantaneous spanwise average at the same streamwise and wall-normal location. The region depicted in the plots is moving downstream to follow the perturbation. The initial condition evolves into an antisymmetric wave packet most clearly seen around the low-speed region, here in the middle of the domain. These spanwise oscillations occur mainly in the upper part of the boundary layer. Comparing Figs. 7(a) and 7(b),

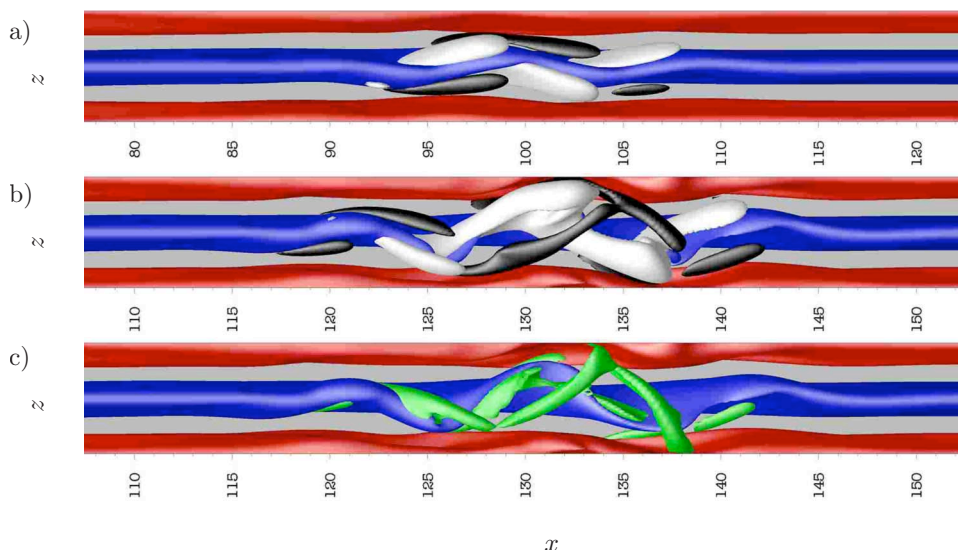


FIG. 8. (Color online) Top view of the early flow development for the nonlinear impulse response. Medium gray (red) and dark gray (blue) isocontours correspond to high- and low-speed streaks (see Fig. 7); white and black isocontours are positive and negative wall-normal velocity at times (a) $t=120$ ($v = \pm 0.02$) and (b) $t=160$ ($v = \pm 0.035$). (c) Light gray (green) isocontours correspond to the λ_2 criterion $\lambda_2 = -0.01$ at time $t=160$.

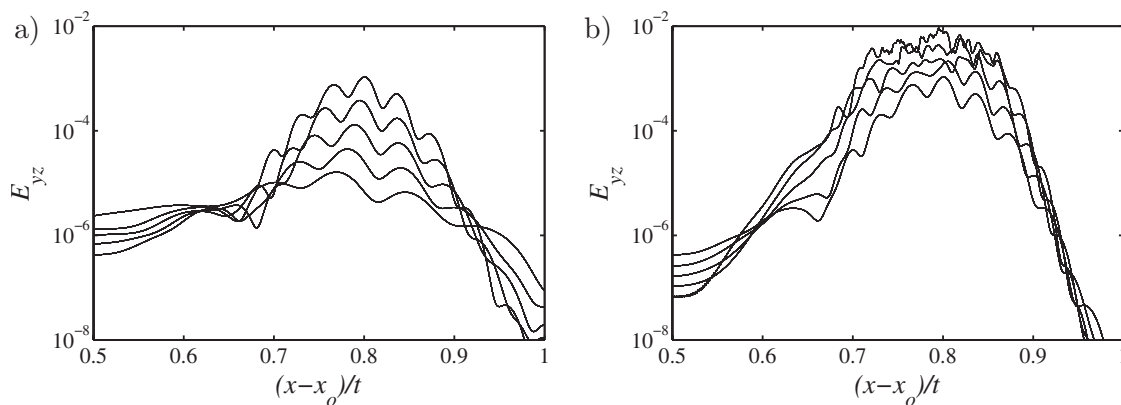


FIG. 9. Spanwise fluctuation energy for the nonlinear impulse response. (a) Early linear evolution $60 < t < 140$ with interval $\Delta t = 20$ and (b) later nonlinear evolution, $140 < t < 220$ with interval $\Delta t = 20$.

the growth in amplitude of the oscillations is clearly visible. Simultaneously, the wave packet is spreading in the streamwise direction; two oscillations can be distinguished at time $t = 120$, while at $t = 160$ the streak presents three oscillations. At later times, Fig. 7(c), the streak is disrupted and a region of turbulent flow ($165 < x < 185$ at $t = 220$) is traveling within a fully steady and laminar streak. This is in agreement with the observation in bypass transition where turbulent flow is seen to be surrounded by regions of laminar streaky flow. The wavelength of the oscillations is found to be of about $11\delta^*$, close to the wavelength of maximum growth rate obtained with the linear computations.

Surfaces of constant wall-normal velocity at the early stage of breakdown are reported in Figs. 8(a) and 8(b), where the underlying streak is also shown to facilitate comparisons. This velocity component appears in antisymmetric patches, as expected from linear sinuous instability analysis. Conversely, the spanwise velocity presents a symmetric distribution with respect to the low-speed streak (not shown here). The amplitude of the fluctuations is growing and the wave packet is spreading as deduced by the streamwise velocity isosurfaces. Positive wall-normal velocity is found to precede the oscillation of the low-speed streak, while negative values are observed after the passage of the low-speed fluid. The regions of positive and negative velocities are both following the streak bending. The vortical structure characteristics of the unstable wave packet are reported in Fig. 8(c). These are found to consist of quasistreamwise vortices alternating in a staggered pattern and following the streak oscillation. The structures are tilted away from the wall in the downstream direction, all in striking similarity with the observation in boundary layers exposed to free-stream turbulence (see next section). It is also interesting to note that as in the case of harmonic forcing,¹⁵ quasistreamwise vortices are both found closer to the wall on the flanks of the (oscillating) low-speed streaks and also in the upper part of the boundary layer. The upper vortices have a similar pattern than the ones closer to the wall, but a different phase with respect to the streak oscillations underneath.

Quantitative data for the evolution of the wave packet are shown in Fig. 9. The figure displays the streamwise variations in the energy of the periodic part of spanwise ve-

locity perturbations integrated over cross-stream planes. The curves are displayed versus the group velocity $(x-x_0)/t$. The data in Fig. 9(a) display early times, where the flow is clearly dominated by the sinuous instability mode, whereas Fig. 9(b) depicts the behavior at later times when the streak is transitional and has broken down to initial turbulent stages. It should be noted that, owing to high perturbation levels at low wavenumbers, it is not possible to perform the Hilbert transform in the streamwise direction²⁷ to regularize the signal from the wave packet in the case of nonlinear flows, see also Ref. 35. Therefore, the energy is characterized by the strong oscillations due to the crest of the waves forming the packet. However, it can be seen that the amplitude of the perturbations grows between the trailing- and leading-edge velocities of the wave packet which can be identified to be about $v^- \approx 0.65$ and $v^+ \approx 0.92$. The strongest perturbations travel at $0.8U_\infty$, as observed from the computation of the linear flow response. At the late nonlinear stages, Fig. 9(b), the growth of the wave packet has saturated as shown by the overlapping of the energy curves pertaining to the latest times. The leading edge of the wave packet, invading regions of laminar flow, is still traveling at the same group velocity, $v^+ \approx 0.92$, while the trailing edge is slowing down once the streak is disrupted. The trailing edge of the turbulent region is traveling at about half the free-stream velocity, $v^- \approx 0.55$.

The streamwise maximum of the perturbation energy integrated over cross-stream planes is displayed versus time in Fig. 10. This quantity is chosen to indicate the growth rate of the most unstable waves, those traveling with a group velocity of about 80% of the free-stream velocity. After the initial transient when the wave packet assumes the sinuous symmetry, the amplification is exponential, linear in the logarithmic plot, with a best-fit growth rate of 0.0255. The value is slightly lower than those observed for a parallel streak of the same amplitude at the inlet ($\omega_i = 0.032$). This can be explained by the fact that the streak amplitude is decaying downstream in the region used for the present simulations. Saturation of the perturbation is observed at later times when the streak has broken down.

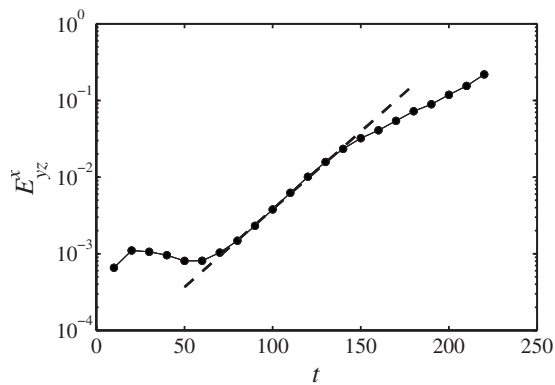


FIG. 10. Temporal energy growth for the nonlinear impulse response. The streamwise maximum of the perturbation energy integrated over cross-stream planes is displayed vs time.

D. Spot precursors in bypass transition

In a boundary layer subject to free-stream turbulence the streak secondary instability is triggered by localized perturbations, most likely those present in the free stream. Therefore, the instability is developing as a localized wave packet. The similarity with the flow structures observed in the transitioning wave packet shows that the secondary-instability mechanism is indeed at work also in bypass transition.

Flow visualizations from spot precursors in a boundary layer subject to free-stream turbulence are now presented. As mentioned in Sec. I, both symmetric and antisymmetric streak oscillations are identified in the experiments and in the numerical simulations, the sinuous modes being the most likely to occur.^{6,10} When compared to the previous results on the breakdown of a steady nonlinearly saturated streak subject to a localized initial perturbation, the figures of this section provide evidence for the role of the streak secondary instability in bypass transition. Despite the noisy environment leading to low-speed streak motions and their finite length, the similarities with the breakdown of a single steady and periodic streak are obvious.

The experimental results are presented first. Five measurement runs could be selected in which an unstable low-speed streak shows a sinuous wavy motion.¹³ A typical sequence from one of these cases obtained with the combined PIV-LIF technique and with the instability present in the measuring domain is displayed in Fig. 11. The two images visualize the sinuous movement of the dye streaklines (background gray scale), while the vectors represent the streamwise and spanwise disturbance components of the instantaneous velocity field. They are obtained by subtracting the

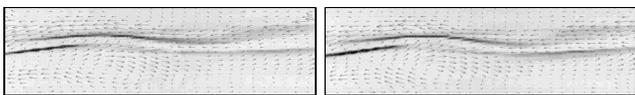


FIG. 11. Typical image sequence obtained with the combined PIV-LIF technique. The vector plot represents the disturbance field, while the gray scale indicated the dye intensity, here black states high dye intensity and white low intensity. $Re_\tau = [1.52 \times 10^5, 1.56 \times 10^5]$. Real aspect ratio. From J. Mans, Ph.D. thesis, Eindhoven University of Technology, 2007; courtesy of Mans and de Lange.

median of the corresponding velocity within the PIV image. The velocity-disturbance field shows the presence of high- and low-speed streaks, with the latter oscillating in a sinuous motion. Vortices in the high-shear region on the flank of the streak can clearly be seen.

An obvious advantage of a numerical study is that once a turbulent spot is observed, the same simulation can be repeated to have access to the full three-dimensional velocity and vorticity fields and the location of the spot formation be traced back in time. Therefore, the type of simulations presented by Brandt *et al.*⁶ have been repeated here to analyze in detail several of the spot precursors observed. Their main feature is the appearance of regions of positive wall-normal and spanwise velocity in a quasiperiodic pattern, located in correspondence to a low-speed region. The streaks generated under free-stream turbulence are not symmetric and the high-frequency perturbations riding on them do not show a clear symmetry either. However, in comparison with the model problems mentioned above, the velocities conserve almost the same pattern with respect to the mean shear of the streaks.

Three-dimensional instantaneous views of six different sinuous spot precursors observed during an integration time of 4000 nondimensional units, corresponding roughly to four passages through the computational domain, are displayed in Figs. 2 and 12. During that integration time, a total of 22 incipient turbulent spots have been observed, corresponding to a specific nondimensional spot birth rate of 1.06×10^{-4} . In the plots, red (medium gray) and blue (dark gray) represent surfaces of constant streamwise velocity perturbation $u' = \pm 0.15$, whereas the green (light gray) structures indicate negative values of λ_2 , the second largest eigenvalue of the Hessian of the pressure, used here to identify vortical structures.¹⁷ The flow features common to all cases displayed [with the exception of Fig. 2(b) which shows a varicose instability] are the spanwise oscillations of the low-speed streak and the presence of quasistreamwise vortices on the flank of the low-speed region. The streak instability appears as a wave packet, with staggered patterns of streamwise vortices consisting of three to five structures. The spatial wavelength of these oscillations is estimated to be between 7 and 11 local displacement thicknesses δ^* . The amplitude of the streaks involved in the instability is estimated according to Eq. (3) to be $A \approx 0.30U_\infty$; locally the negative disturbance velocity $-u'$ can reach values in excess of $0.35U_\infty$. On the other hand, streaks that do not experience instability and subsequent turbulent breakdown are rarely of amplitude larger than $A = 0.2U_\infty$.

The flow structures in the fourth plot, Fig. 12(d), and Fig. 2(b) are those most similar to the nonlinear impulse response presented in the previous section [e.g., Fig. 8(c)]. The low-speed streak in the first plot Fig. 12(a) is highly asymmetric as observed by the fact that a region of high-speed fluid is found only on its left side. As a consequence, the following instability is also asymmetric and the quasistreamwise vortices observed are only those bending in the positive spanwise direction. The second plot, Fig. 12(b), depicts the effect of the streak finite length. It can be seen in the figure that the instability is triggered at the head of an

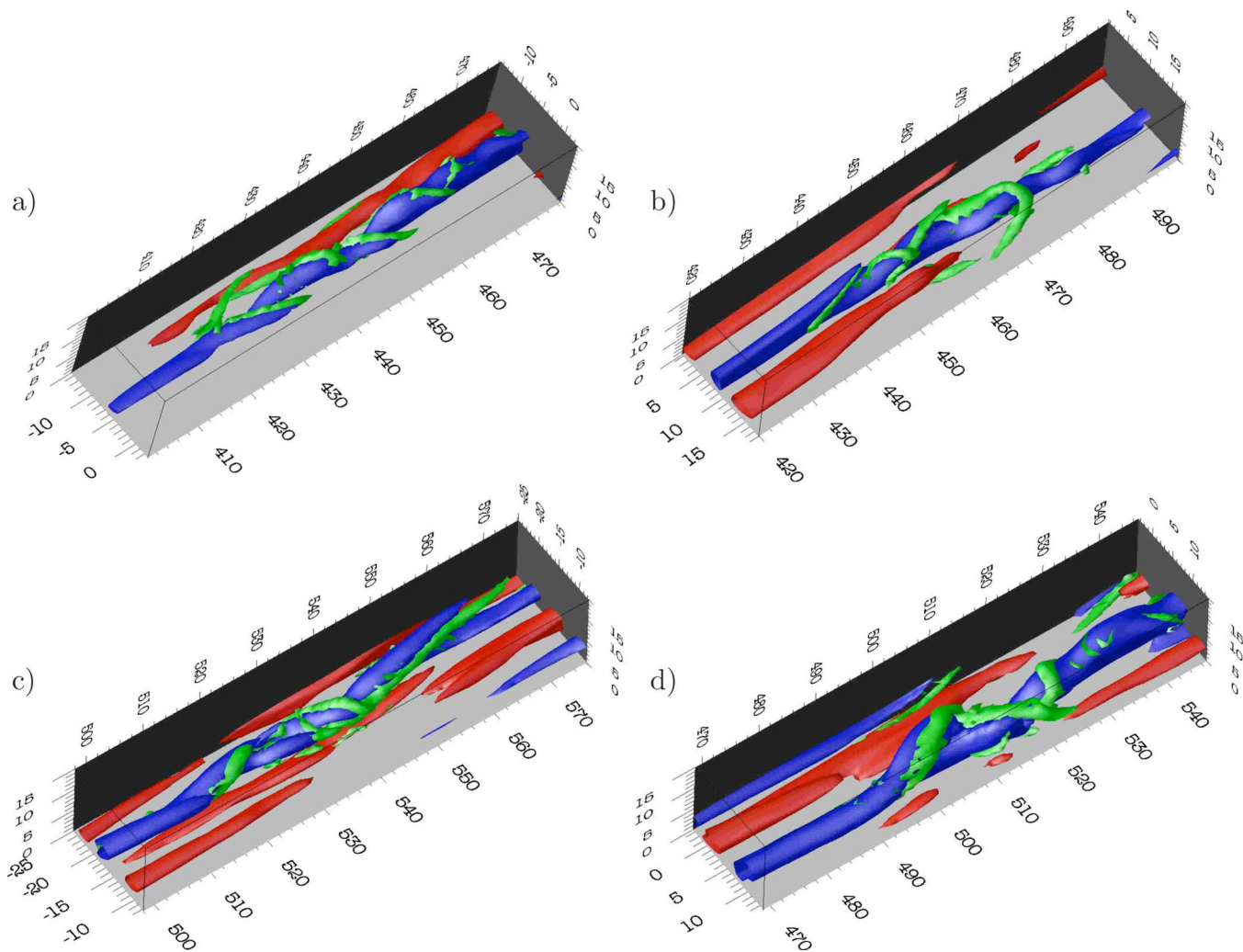


FIG. 12. (Color online) Three-dimensional visualizations of sinuous streak instability prior to the formation of a turbulent spot. Isocontours of positive and negative streamwise disturbance velocities $\pm u' = 0.15$ in medium (red) and dark gray (blue), respectively, and surfaces of the λ_2 vortex identification criterion ($\lambda_2 = -0.002$) in light gray (green).

incoming region of high-momentum fluid: as this approaches the low-speed streak on its left a region of high spanwise shear is forming and here the instability is first seen. Motivated by these observations, Brandt and de Lange³⁶ have recently investigated numerically the interaction between optimal streaks assumed periodic but of finite streamwise length. These authors observe that this interaction is able to trigger the streak breakdown and that the following flow structures are very similar to those in bypass transition. Finally, we note that the remaining instability, Fig. 12(c), is characterized by short high-frequency oscillations around $x = 530$ as well as low-frequency meandering further downstream ($540 < x < 570$). Long sinuous oscillations of the low-speed streak were also reported by Mans *et al.*¹⁰

IV. CONTINUOUS MODE TRANSITION

In recent publications, Zaki and Durbin² and Durbin and Wu¹² advocated a different mechanism for the breakdown of the streaks in boundary layers under free-stream turbulence; namely, a Kelvin–Helmholtz instability in the upper part of the boundary layer which they claim is triggered by interac-

tions between the free-stream eddies and the lifted low-speed streaks. Such an instability would be triggered locally in the upper part of the boundary layer. On the other hand, the secondary instability of the streaks as discussed in the previous sections involves a wave packet closely connected to the streak itself; initiated of course by the free-stream turbulence. In that respect the triggering of the instability on the streak is different. Zaki and Durbin further proposed a model of bypass transition based on the interaction of only a few free-stream modes which exhibited this specific breakdown pattern. In particular, these authors show that laminar-turbulent transition of a zero-pressure gradient boundary layer can be triggered with only two modes of the continuous spectrum of the Orr–Sommerfeld/Squire equations³⁷ imposed at the inlet, provided that one of these modes is of low temporal frequency and the other of sufficiently high frequency.

We have carried out a simulation using this model with our own numerical code and postprocessing tools. In summary, we have obtained virtually the same results as the published results,² however, our conclusions regarding the domi-

TABLE I. Parameters for the various numerical simulations presented. The Reynolds number $Re_{\delta_0^*}$ denotes the location of the inflow of the computational domain, which is chosen larger for the cases involving the study of the instability only.

Case	$Re_{\delta_0^*}$	Domain size	Resolution
Linear impulse response ^a	1047	$1200 \times 10 \times 5.8$	$1024 \times 97 \times 32$
Nonlinear impulse response	1044	$318 \times 9 \times 5.8$	$1440 \times 97 \times 72$
DNS bypass transition ^b	300	$1000 \times 60 \times 50$	$1024 \times 121 \times 72$
Zaki–Durbin model	350	$1000 \times 60 \times 46$	$720 \times 193 \times 120$

^aReference 27.

^bReference 6.

nant instability and breakdown mechanism are different. These findings will be discussed next.

A. Model description and parameter settings

DNSs were performed using the spectral numerical method described in Sec. II. The Reynolds number at the inlet is $Re_{\delta_0^*}=350$, corresponding to $Re_x=41\,360$, where $Re_x=U_\infty x/\nu$. Further details of the simulation setup are given in Table I.

The modes to be used as inflow condition are solutions to the linearized Orr–Sommerfeld/Squire operators and are characterized by a real spanwise wavenumber β_N , temporal frequency ω_N , and a wall-normal wavenumber γ_N which reflects the oscillatory behavior of the modes far away from the wall. The complex eigenvalue α_N is computed by a numerical procedure discussed in, e.g., Refs. 4, 6, and 37. Note that the modes of the continuous spectrum are all decaying in the streamwise direction [i.e., $\Im(\alpha) > 0$], with modes of largest γ_N being the most damped.

Two modes similar to Zaki and Durbin² have been chosen, each representing either a low-frequency mode (mode A) or a high-frequency mode (mode B). Table II lists the relevant parameters together with their eigenvalue and amplitude. Note that for each mode A and B both the contributions of $+\beta_N$ and $-\beta_N$ are considered; both the positive and negative contributions are referred to as one mode in the following. The eigenfunctions of the wall-normal velocity component \hat{v} pertaining to these modes are depicted in Fig. 13. The maximum value of the wall-normal velocity component of the eigenfunctions \hat{v}_{\max} is normalized to 2% and 1% of the free-stream velocity U_∞ , respectively. The relative temporal phase of modes A and B is chosen randomly. As can be seen in Fig. 13 the low-frequency mode A is, in fact, able to penetrate deep into the boundary layer, inducing oscillations even close to the wall. On the other hand, mode B is not able to overcome the boundary-layer shear,³⁸ reducing

its amplitude to essentially zero below $y \approx 2\delta^*$. Note that the terms low and high frequencies are related to temporal frequency, not spatial wavenumber. In particular, mode A has a larger wall-normal wavenumber γ_N than mode B, but is still able to penetrate deeper.² For both modes A and B, the streamwise fluctuation \hat{u} is approximately five times smaller than the wall-normal fluctuation; the spanwise fluctuation \hat{w} for mode A is of about the same magnitude as \hat{v} , whereas for mode B \hat{w} and \hat{u} are comparable.

In order to impose modes A and B as inflow conditions in our numerical simulation, a forcing is added in the fringe region [see Sec. II and Eq. (1)] toward the laminar Blasius solution with the superimposed harmonic disturbances of the form

$$\mathbf{u}_d = \sum_{\text{modes A,B}} \hat{\mathbf{u}}_N e^{\pm i\beta_N z + i\alpha_N x - i\omega_N t}. \quad (5)$$

Similarly as described by Brandt *et al.*⁶ the inflow perturbation in expansion (5) is damped to zero by a smooth step function above a wall-normal position $y > 40\delta_0^*$. The boundary condition imposed on the top of the domain is a Neumann condition on all velocity components. The streamwise wavenumber α_N is used in the expression above since the modes are forced over the whole length of the fringe region upstream of the inlet location. The wall-normal wavenumber γ_N enters implicitly through the eigenfunction shape. Note that in addition to the temporal phase of the two mode pairs a spanwise displacement between modes A and B can be introduced. This spanwise phase can be used to shift the spanwise location of the most intense interaction between the two modes. This will be discussed further below.

B. Simulation results

As a first step, several simulations have been performed with only one of the two modes A and B forced at the inlet. Corresponding results are presented in Fig. 14 for the streamwise rms velocity fluctuations. As expected and discussed in, e.g., Refs. 2 and 38, mode A immediately gives rise to strong streamwise perturbation, the boundary-layer streaks. These streaks are formed due to the well-known lift-up effect,³⁹ after which a weak wall-normal displacement in a shear layer dominated by spanwise vorticity may cause large velocity differences in the streamwise direction. The streaks have their maximum amplitude at about half the boundary-layer height, and their rms amplitude first grows, and after $x \approx 200$ (corresponding to $Re_x \approx 110\,000$) viscous decay sets in without causing transition to turbulence. Instantaneously, the streak amplitude defined according to Eq. (3) reaches 35% of the free-stream velocity U_∞ at $x=500$. The

TABLE II. Parameters of the low-frequency (A) and high-frequency (B) modes of the continuous spectrum of the Orr–Sommerfeld/Squire equation. Note that modes A and B each contains both $\pm\beta$ contributions. The spanwise width of the domain is $L_z=46$.

Mode	\hat{v}_{\max}	ω_N	α_N	β_N	γ_N
A	2%	0.0112	$0.0112 + 0.002\,56i$	$\pm 0.683 = 5 \cdot 2\pi/L_z$	0.656
B	1%	0.225	$0.225 + 0.003\,94i$	$\pm 1.09 = 8 \cdot 2\pi/L_z$	0.367

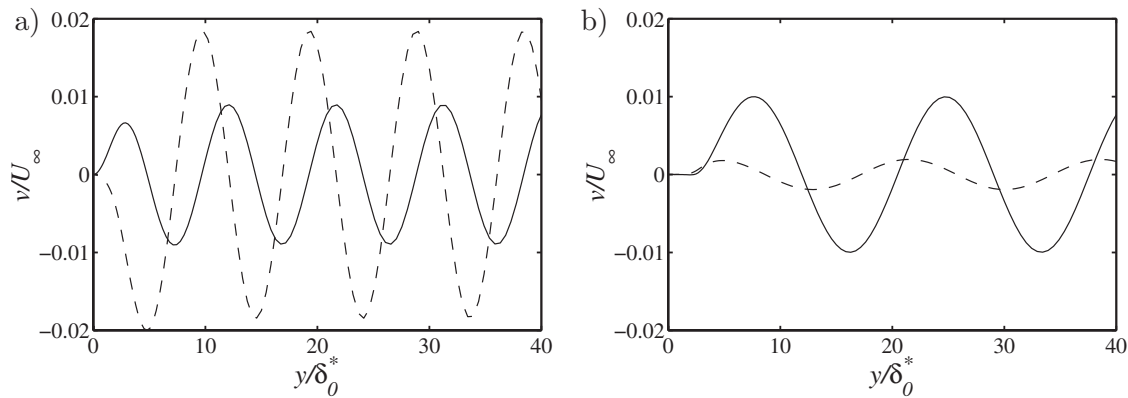


FIG. 13. Complex eigenfunctions \hat{v} of the wall-normal velocity component pertaining to modes A and B used together with the Zaki–Durbin model problem, at the inlet $x=0$. (—) Real part; (---) imaginary part. (a) Penetrating low-frequency mode A. (b) Sheltered high-frequency mode B.

streaks have the spacing dictated by the spanwise wavenumber of the corresponding continuous mode A, i.e., with the present setting five streaks in the domain with width L_z . Additionally, the streaks are unsteady, i.e., the low- and high-speed streaks alternate in spanwise position every $T = \pi/0.0112 = 280.5$ time units. Similar results have also been shown in Ref. 2.

If, on the other hand, only mode B with higher temporal frequency ω_N is forced at the inlet, no streaks can be detected in the resulting flow fields, i.e., the fluctuations are not able to fully enter the sheared boundary layer. However, close to the boundary-layer edge (above local $\delta^* \approx 2$) a fluctuation maximum, albeit much smaller than for case A, can be detected. This is due to the displacement effect of the spatially growing boundary layer coupled with the sheltering of the free-stream fluctuations. As with only mode A, viscous decay is causing the disturbances inside and outside the boundary layer to decay, preventing the flow from undergoing transition.

In a next step, both modes A and B are imposed at the inlet in a similar fashion as done in Ref. 2. As mentioned above, the amplitudes of the eigenfunctions pertaining to modes A and B are 2% and 1%, respectively. The measured rms amplitudes at the inlet of the domain $x=0$ are shown in Fig. 15 for modes A, B, and their combination. Modes A and B are essentially mutually orthogonal, so the combined rms

amplitude corresponds to the sum of the fluctuation energies of the two individual contributions. However, the actual maximum amplitude is mainly dominated by mode A and is $v_{\text{rms}} \approx 2\%$. Note that the amplitude employed here is slightly lower than the one reported by Zaki and Durbin.²

When the two modes are superposed, an additional relative displacement in the lateral z direction can be introduced, allowing a shift of the spanwise position of the most intense interaction between the modes. In particular, the maxima of the high-frequency mode B can be shifted to coincide with a high-speed streak (generated by mode A), a low-speed streak, or somewhere in between. Since the instability described below will always appear on top of a low-speed streak leaving the high-speed streaks virtually unaffected, centering mode B on the high-speed streaks will result in a lateral symmetric breakdown pattern with symmetry plane in the high-speed streak. If, on the other hand, mode B is focused on the low-speed streak, no spanwise symmetry will arise. However, the resulting statistical quantities and the instantaneous flow visualizations do not show any differences regarding the instability mechanism. Therefore, it was decided to center mode B on the low-speed streak located at $z = -4.6$, resulting in nonsymmetric velocity fields similar as those presented by Zaki and Durbin.²

In contrast to only imposing one mode at the inlet, the interaction of the two modes leads to laminar-turbulent tran-

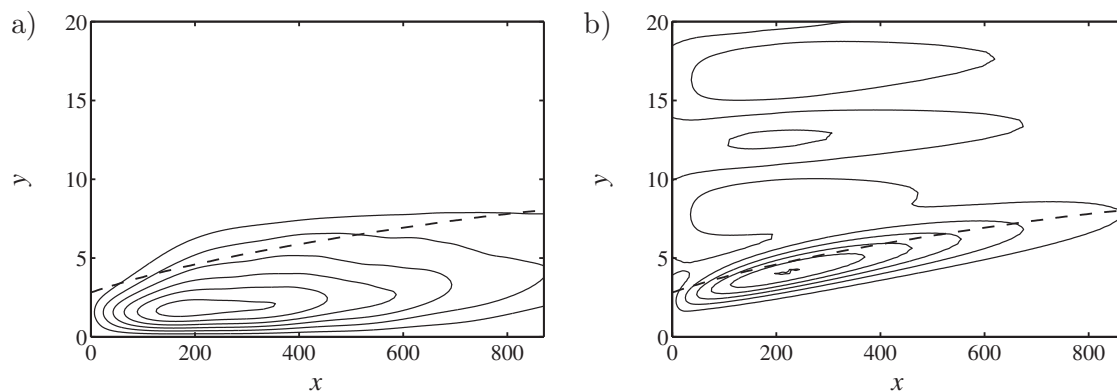


FIG. 14. Streamwise velocity fluctuation u_{rms} in a x/y -plane for the penetrating mode A and nonpenetrating mode B. (---) δ_{99} boundary-layer thickness. Contour spacing and starting level for mode A: 0.025; for the nonpenetrating mode B: 0.0005.

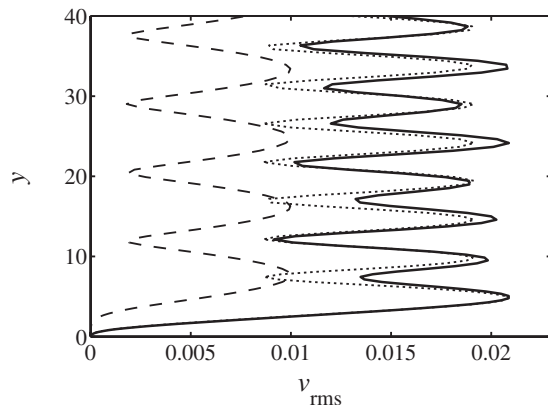


FIG. 15. Wall-normal fluctuation v_{rms} at $x=0$ for (\cdots) penetrating mode A, ($-\ - -$) nonpenetrating mode B, and ($—$) both modes A and B together.

sition within the computational box. The skin-friction coefficient c_f for the various simulations is presented in Fig. 16 together with analytical correlations for both the laminar and turbulent regimes. One can clearly see that up to $x \approx 400$ ($Re_x \approx 180\,000$) the skin friction essentially follows the values obtained with only mode A, showing a slightly increased velocity wall gradient due to the presence of the strong boundary-layer streaks. Note that the presence of mode B alone is not affecting the skin friction at all, i.e., it remains at the laminar value. However, more downstream $x > 400$ the onset of transition is visible due to the increase in the averaged skin-friction coefficient; at $x=800$ the well-known overshoot of c_f over the turbulent value can be observed.

Instantaneously, the flow is dominated by the intermittent appearance of turbulent spots, which convect and grow downstream until the full span of the domain is fully turbulent. This behavior can be seen in the instantaneous skin-friction coefficient (Fig. 16, thin solid line, only spatially averaged without temporal mean). In Fig. 17 the wall-normal velocity component is displayed in a wall-parallel plane inside the boundary layer, clearly showing the streaks in the upstream part of the domain, the appearance of a turbulent

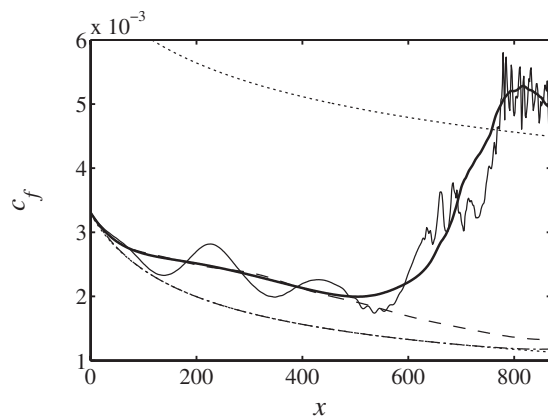


FIG. 16. Skin-friction coefficient c_f for various cases. ($—$) Temporally and spatially averaged simulation results; ($—$) instantaneous for combination of modes A and B. ($-\ - -$) and ($-\ \cdot -$) only penetrating (a) and nonpenetrating (b) modes, respectively. (\cdots) Laminar [Blasius, $c_f = (2/3)Re_x^{-0.5}$] and turbulent ($c_f \approx 0.0576 Re_x^{-0.2}$) correlations. Note that the laminar correlation virtually collapses with c_f of mode B.

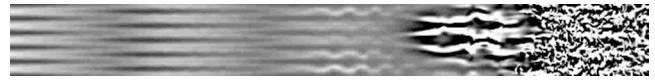


FIG. 17. Top view of instantaneous wall-normal velocity v at fixed wall-normal distance $y=2\delta_0^*$, ranging from -0.02 (black) to 0.02 (white). Plotted range $x=[0,900]$, $z=[23,-23]$, at relative time $t=356$.

spot, and the fully turbulent downstream region close to the outflow. This intermittent behavior is very similar to what has been observed for bypass transition, from both experiments^{8,9} and simulations.^{4,6}

As pointed out by Durbin and Wu¹² a two-dimensional plan view cannot give all the details necessary to understand and interpret the various phenomena involved in flow instability and breakdown; sometimes such a view can even be deceiving. Therefore, in Fig. 18 three-dimensional instantaneous visualizations are shown for three time instants during breakdown due to continuous mode interaction. Boundary-layer streaks are visualized with isocontours for positive and negative streamwise disturbance velocities u' , and vortical structures are shown using the λ_2 vortex identification criterion.¹⁷

Similar as in Zaki and Durbin,² also instantaneous two-dimensional cuts in a x/y -plane showing contours of the streamwise velocity fluctuation are given in Fig. 19 for three distinct times during transitional breakdown. The spanwise position of the cuts is $z=-4.6$, i.e., corresponding to a cut through the low-speed streak in the center of the emerging turbulent spot (see comments on the spanwise phase of the mode pairs above).

In the first frame of the three-dimensional views (Fig. 18), one can clearly appreciate a spanwise oscillation of the low-speed streaks, each of the wiggles closely connected to an intense vortical structure (zigzag pattern of λ_2) on its top. The sense of rotation is such that in a region where two vortices are approaching each other fluid is lifted away from the wall from the region in between. Following Andersson *et al.*²⁶ this pattern can be categorized as a subharmonic sinusoidal streak instability. Note that the temporal frequency of the secondary streak instability is imposed by the high-frequency mode B. Qualitatively comparing these flow structures to the visualization in Figs. 7 and 8 pertaining to the nonlinear impulse response on steady streaks shows a striking resemblance. In particular, at a fixed time the regions of intense negative disturbance velocity (i.e., the isocontours of negative disturbance velocity visualizing the three-dimensional shape of the low-speed streak) show larger spanwise amplitudes with increasing wall distance; the high-speed streaks in between are hardly affected by these oscillations.

The later frames in this sequence (Fig. 18) show the evolution of the wave packet into increasingly complex nonlinear states. In particular, the amplitude of the spanwise oscillations increases with time (and downstream distance) until the amplitudes are so strong that the vortices riding on top of the low-speed streaks actually connect above the high-speed streak, forming structures which appear similar to classical hairpin vortices. The associated roll ups of the shear layer then proceed on these individual heads of hairpins,

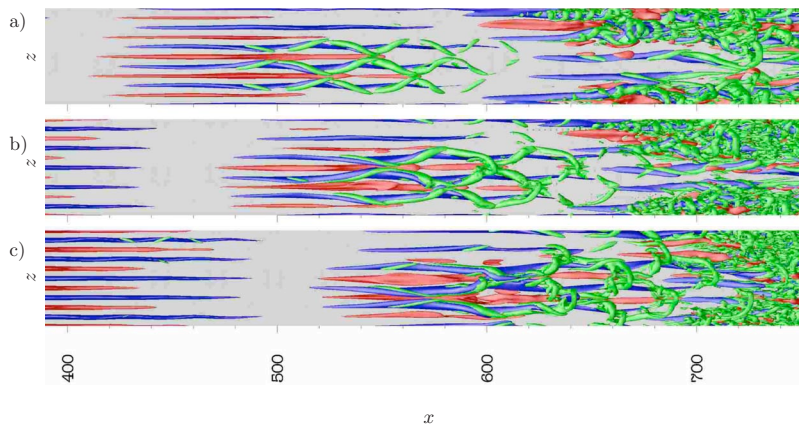


FIG. 18. (Color online) Three-dimensional top view of the flow structures pertaining to the Zaki–Durbin model problem. Isocontours of $u' = \pm 0.16$ (medium and dark gray, red, and blue) and $\lambda_2 = -0.001$ (light gray, green). Relative times $t=141$, $t=211$, and $t=281$. True aspect ratio, spanwise range $z = [-23, 23]$.

leading to increasingly complex flow patterns and the subsequent generation of smaller scales. Eventually, a turbulent spot is born.

Due to the spanwise and temporal scales chosen for the two modes, A and B, the aforementioned mode interactions will always take place at two distinct spanwise positions, i.e., for the present case at $z = -4.6$ and $z = 18.4$, alternating periodically with temporal separation of $\pi/\omega_A \approx 281$ time units. Consequently, in the last frame of Fig. 18 one can already spot the growing (weak) wave packet on the low-speed streak positioned at $x=440$ and $z=18.4$.

If one considers the vertical cuts in the streamwise direction, Fig. 19, the three-dimensional zigzag structure of the traveling instability cannot be seen. The obvious cat-eye pattern, which intensifies with later times, looks similar to a type of Kelvin–Helmholtz instability, as discussed in Ref. 2. However, the complete three-dimensional views of the structures associated with the breakdown to turbulence clearly show a more intricate origin of the instability. Rather than just a local breakdown due to inflectional profiles and triggered by free-stream modes, it becomes clear that we are

dealing with finite amplitude structures caused by a developing sinuous secondary instability of the underlying streaks.

C. Comparison of characteristics of breakdown

In Table III we have collected the characteristics of the sinuous breakdown for the various cases reported in the previous sections. Whereas for the inviscid instability and the linear impulse response, exact values can be given, the other numbers need to be estimated from the respective simulations and experiments. Note that for the Zaki–Durbin model problem² the wavelength of the streak secondary instability is imposed by the *a priori* chosen wavenumber of the high-frequency mode (see the previous section), which explains its apparently different value.

The data collected in the table clearly show that the various approaches to secondary instability on streaks, ranging from inviscid instability over impulse responses on parallel and spatially developing streaks, essentially give the same results as full simulations and experiments of bypass transi-

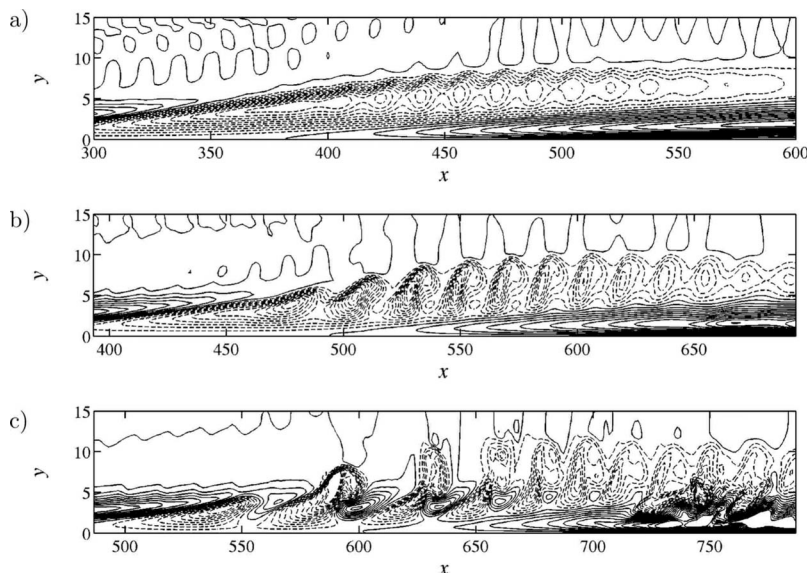


FIG. 19. Wall-normal cuts displaying contours of the streamwise disturbance velocity for the Zaki–Durbin model problem at relative times $t=0$, $t=141$, and $t=281$. Spanwise position $z = -4.6$, contour spacing of 0.025, negative values are denoted by dashed lines.

TABLE III. Comparison of breakdown characteristics for sinuous streak breakdown. The wavelength is in units of the local displacement boundary-layer thickness δ^* , the velocities of the free-stream velocity U_∞ , and the growth rate of U_∞/δ^* . The three values for the propagation velocity relate to the velocity of the tail, center, and leading edge of the instability, respectively.

Sinuous instability	Wavelength	Growth rate	Propagation velocity		
Inviscid instability	10.4	0.035			
Linear impulse	10.4	0.032	0.65	0.8	0.95
Nonlinear impulse	11	0.025	0.55	0.8	0.95
Zaki–Durbin model	20		0.55	0.85	0.95
KTH simulations	7–11			0.85	
TU/e experiments	9–16	0.01		0.8	

tion; not only with respect to flow visualizations but also concerning characteristic measures of the involved instability mechanism.

V. CONCLUSIONS

Recent theoretical, numerical, and experimental investigations of bypass transition in a zero-pressure gradient boundary layer under free-stream turbulence have been revisited. New material was also presented which clarifies the role of the streaks and their breakdown in bypass transition. In all of the flow cases considered, in particular, temporal secondary instability of a steady streak, impulse responses both on a parallel and a spatially developing streak, a model of bypass transition, and bypass transition itself, similar characteristics of the streak breakdown have been found. Namely, the streaks break down due to a sinuous secondary instability with a wavelength about an order of magnitude larger than the local boundary-layer displacement thickness, a growth rate of the order of 1% of the free-stream velocity over the boundary-layer thickness and a group velocity of about 0.8 of the free-stream velocity. The secondary instability manifests itself in all cases as a growing wave packet situated on the low-speed streak, increasing in magnitude as it is dispersing in the streamwise direction. After a sufficiently long period of growth the flow locally breaks down and a turbulent spot is formed. Thus the streak secondary-instability process for the generation of turbulent spots is clearly shown. These findings are in contrast to those presented recently by Durbin and Wu,¹² who instead proposed a Kelvin–Helmholtz instability mechanism for the breakdown, both in their model of bypass transition and in bypass transition itself. Their interpretation seems to originate from the fact that they are only considering two-dimensional plane views of the flow and have not considered three-dimensional surfaces of, e.g., low-speed streaks and their associated vortical structures. The corresponding three-dimensional views and associated animations (not reported here) clearly support the view presented in the present paper.

Although the origin of the sinuous breakdown now is clarified, the receptivity issue is still an open question. It is the view of the authors of the present paper that it most likely is disturbances in the free-stream which cause the triggering of the high-frequency instabilities as shown by the stochastic analysis in Ref. 31. Since the low-speed streaks

extend quite high in the boundary layer, they are susceptible to these types of perturbations. However, other triggering mechanisms should also be considered, e.g., acoustic waves (pressure fluctuations).

In addition, there is a need to further study the varicose breakdown, which is also seen to be a cause of the breakdown in certain low-speed streaks. However, this type of breakdown is not as common as the sinuous one discussed here. For further discussion of this type of breakdown and its origin, the reader is referred to the recent work of Brandt and de Lange.³⁶

- ¹P. Andersson, M. Berggren, and D. S. Henningson, “Optimal disturbances and bypass transition in boundary layers,” *Phys. Fluids* **11**, 134 (1999).
- ²T. Zaki and P. Durbin, “Mode interaction and the bypass route to transition,” *J. Fluid Mech.* **531**, 85 (2005).
- ³D. S. Henningson and P. J. Schmid, “Vector eigenfunction expansions for plane channel flows,” *Stud. Appl. Math.* **87**, 15 (1992).
- ⁴R. G. Jacobs and P. Durbin, “Simulations of bypass transition,” *J. Fluid Mech.* **428**, 185 (2001).
- ⁵P. E. Roach and D. H. Brierley, “The influence of a turbulent freestream on zero pressure gradient transitional boundary layer development, part I: Test cases T3A and T3B,” in *Numerical Simulation of Unsteady Flows and Transition to Turbulence*, edited by O. Pironneau, W. Rodi, I. L. Ryhming, A. M. Savill, and T. V. Truong (Cambridge University Press, Cambridge, UK, 1990), pp. 319–347.
- ⁶L. Brandt, P. Schlatter, and D. S. Henningson, “Transition in boundary layers subjected to free-stream turbulence,” *J. Fluid Mech.* **517**, 167 (2004).
- ⁷S. Nagarajan, S. K. Lele, and J. H. Ferziger, “Leading-edge effects in bypass transition,” *J. Fluid Mech.* **572**, 471 (2007).
- ⁸M. Matsubara and P. H. Alfredsson, “Disturbance growth in boundary layers subjected to free-stream turbulence,” *J. Fluid Mech.* **430**, 149 (2001).
- ⁹J. Mans, E. C. Kadijk, H. C. de Lange, and A. A. van Steenhoven, “Breakdown in a boundary layer exposed to free-stream turbulence,” *Exp. Fluids* **39**, 1071 (2005).
- ¹⁰J. Mans, H. C. de Lange, and A. A. van Steenhoven, “Sinuous breakdown in a flat plate boundary layer exposed to free-stream turbulence,” *Phys. Fluids* **19**, 088101 (2007).
- ¹¹P. J. Schmid and D. S. Henningson, *Stability and Transition in Shear Flows* (Springer, New York, 2001).
- ¹²P. Durbin and X. Wu, “Transition beneath vortical disturbances,” *Annu. Rev. Fluid Mech.* **39**, 107 (2007).
- ¹³J. Mans, “Streak development and breakdown during bypass transition,” Ph.D. thesis, Eindhoven University of Technology, 2007.
- ¹⁴Y. A. Litvinenko, V. G. Chernoray, V. V. Kozlov, L. Loef Dahl, G. R. Grek, and H. Chun, “Nonlinear sinusoidal and varicose instability in the boundary layer,” *Thermophys. Aeromechanics* **11**, 329 (2004).
- ¹⁵L. Brandt and D. S. Henningson, “Transition of streamwise streaks in zero-pressure-gradient boundary layers,” *J. Fluid Mech.* **472**, 229 (2002).

- ¹⁶V. G. Chernoray, A. V. Dovgal, V. V. Kozlov, and L. Loeffdahl, "Experiments on secondary instability in a swept-wing boundary layer," *J. Fluid Mech.* **534**, 295 (2005).
- ¹⁷J. Jeong and F. Hussain, "On the identification of a vortex," *J. Fluid Mech.* **285**, 69 (1995).
- ¹⁸M. Chevalier, P. Schlatter, A. Lundbladh, and D. S. Henningson, "SIMSON: A pseudo-spectral solver for incompressible boundary layer flows," KTH Stockholm Technical Report No. TRITA-MEK 2007:07, 2007.
- ¹⁹F. P. Bertolotti, T. Herbert, and P. R. Spalart, "Linear and nonlinear stability of the Blasius boundary layer," *J. Fluid Mech.* **242**, 441 (1992).
- ²⁰M. Ren, C. C. M. Rindt, and A. A. van Steenhoven, "Experimental and numerical investigation of the vortex formation process behind a heated cylinder," *Phys. Fluids* **16**, 3103 (2004).
- ²¹R. N. Kieft, C. C. M. Rindt, A. A. van Steenhoven, and G. J. F. van Heijst, "On the wake structure behind a heated horizontal cylinder in cross-flow," *J. Fluid Mech.* **486**, 189 (2003).
- ²²P. S. Klebanoff, "Effect of free-stream turbulence on the laminar boundary layer," *Bull. Am. Phys. Soc.* **10**, 1323 (1971).
- ²³J. M. Kendall, "Experimental study of disturbances produced in a pre-transitional laminar boundary layer by weak free-stream turbulence," AIAA Paper No. 85-1695, 1985.
- ²⁴K. J. A. Westin, A. V. Boiko, B. G. B. Klingmann, V. V. Kozlov, and P. H. Alfredsson, "Experiments in a boundary layer subject to free-stream turbulence: Part I. Boundary layer structure and receptivity," *J. Fluid Mech.* **281**, 193 (1994).
- ²⁵M. Matsubara, A. A. Bakchinov, J. H. M. Fransson, and P. H. Alfredsson, "Growth and breakdown of streaky structures in boundary layer transition induced by free stream turbulence," in *Proceedings of the IUTAM Symposium*, Sedona, AZ, 1999 (Springer, Berlin, 2000), p. 371.
- ²⁶P. Andersson, L. Brandt, A. Bottaro, and D. S. Henningson, "On the breakdown of boundary layers streaks," *J. Fluid Mech.* **428**, 29 (2001).
- ²⁷L. Brandt, C. Cossu, J.-M. Chomaz, P. Huerre, and D. S. Henningson, "On the convectively unstable nature of optimal streaks in boundary layers," *J. Fluid Mech.* **485**, 221 (2003).
- ²⁸J. Hoepffner, L. Brandt, and D. S. Henningson, "Transient growth on boundary layer streaks," *J. Fluid Mech.* **537**, 91 (2005).
- ²⁹W. Schoppa and F. Hussain, "Coherent structure generation in near-wall turbulence," *J. Fluid Mech.* **435**, 57 (2002).
- ³⁰L. Brandt, "Numerical studies of bypass transition in the Blasius boundary layer," Ph.D. thesis, KTH Stockholm, 2003.
- ³¹J. Hoepffner and L. Brandt, "Stochastic approach to the receptivity problem applied to bypass transition in boundary layers," *Phys. Fluids* **20**, 024108 (2008).
- ³²D. S. Henningson, A. Lundbladh, and A. V. Johansson, "A mechanism for bypass transition from localized disturbances in wall-bounded shear flows," *J. Fluid Mech.* **250**, 169 (1993).
- ³³K. H. Bech, D. S. Henningson, and R. A. W. M. Henkes, "Linear and nonlinear development of localized disturbances in zero and adverse pressure gradient boundary layers," *Phys. Fluids* **10**, 1405 (1998).
- ³⁴K. S. Breuer and J. H. Haritonidis, "The evolution of a localized disturbance in a laminar boundary layer: Part I. Weak disturbances," *J. Fluid Mech.* **220**, 569 (1990).
- ³⁵I. Delbende and J.-M. Chomaz, "Nonlinear convective/absolute instabilities of parallel two-dimensional wakes," *Phys. Fluids* **10**, 2724 (1998).
- ³⁶L. Brandt and H. C. de Lange, "Streak interactions and breakdown in boundary layer flows," *Phys. Fluids* **20**, 024107 (2008).
- ³⁷C. E. Grosch and H. Salwen, "The continuous spectrum of the Orr-Sommerfeld equation: Part I. The spectrum and the eigenfunctions," *J. Fluid Mech.* **87**, 33 (1978).
- ³⁸R. G. Jacobs and P. Durbin, "Shear sheltering and the continuous spectrum of the Orr-Sommerfeld equation," *Phys. Fluids* **10**, 2006 (1998).
- ³⁹M. T. Landahl, "A note on an algebraic instability of inviscid parallel shear flow," *J. Fluid Mech.* **98**, 243 (1980).